AirCargoChallenge 2022

Technical Report

Team #21

JetStream

JET STREAM

Table of contents

Table of acronyms

a – maximum surface deflection

C_l – lift coefficient

C_{lTO} - Lift coefficient (at take-off)

C_{lF} - Lift coefficient (during the flight)

Cx - drag coefficient

l_s - mean control surface cord

L-take off distance

L_s – mean geometric wing cord

M - control surfaces moment

MAC – Mean Aerodynamic Chord

MTOW – Maximum Take-Off

Px – drag force

Pz - lift force

R/C – the rate of climb

Re- Reynolds number

S - lifting surface

S_a - control surface area

T-thrust

V – take-off velocity

V_{cr} - Cruise speed

V_{max}- maximum velocity

W-weight

μ- Coefficient of friction

ν – Kinematic viscosity

ρ - air density

λ – aspect ratio

1. Introduction

This report was written by the JetStream group from Wroclaw University of Science and Technology, which brings together students who are specialized in fields such as mechanical engineering, mechatronics, and aviation engineering. This report aims to present the process of design and testing of an unmanned aircraft built to participate in the Air Cargo Challenge 2022 competition. Everything written here is followed by almost 2 years of project development involving significant changes in team composition, new manufacturing techniques, and delays caused by COVID-19.

2. Project management

2.1. Management and risk analysis

In 2020, two groups were formed, to compete with each other in creating the best design. As time and the pandemic progressed, one of the group's members left the main team and a competition hold was announced. In 2022, a beginner group was designated by older team members to finish the project under their supervision. From human resources perspective, this caused unnecessary delays, but aircraft design quality stayed unaffected. A decision was made to follow the V-model development plan (Figure 1), which is derived from the waterfall methodology.

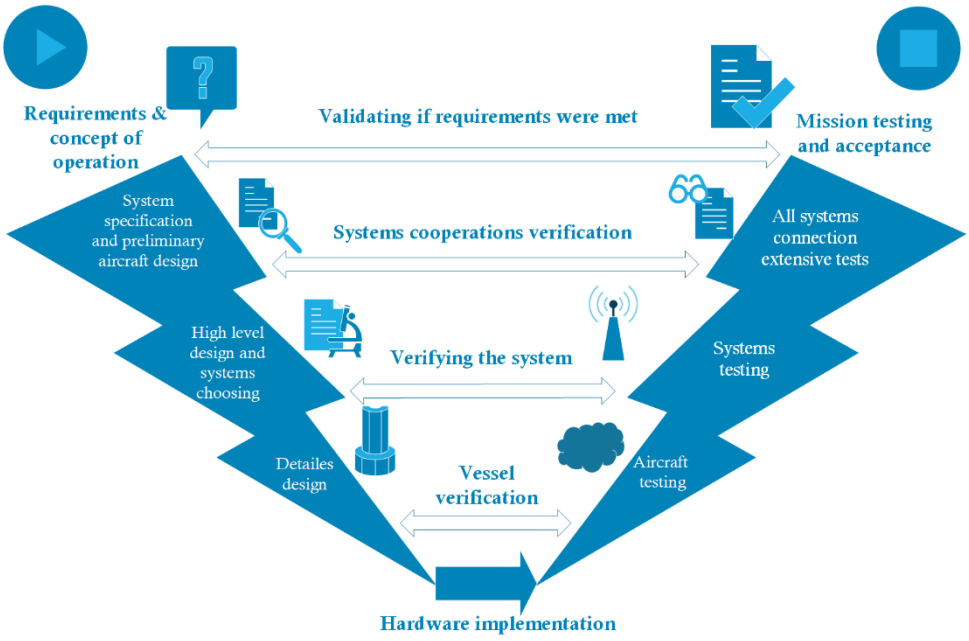

Figure 1 V-model development process.

The team captain defined specific tasks, which were controlled and assigned using an electronic Kanban board provided with the ClickUp app. These were discussed during weekly team meetings. Additionally, the strict time control was introduced using a critical path as shown in Section 2.3. This approach enabled clear task progress recognition and project stall prediction which led to flexible work planning and assignment of suitable resources for the management and precise scope of the work to be done, costs, necessary assets, and knowledge for other team members. For recognition of the risk levels occurring during project phases, the Impact Matrix was prepared, so the Team could focus more on the critical areas (Figure 2).

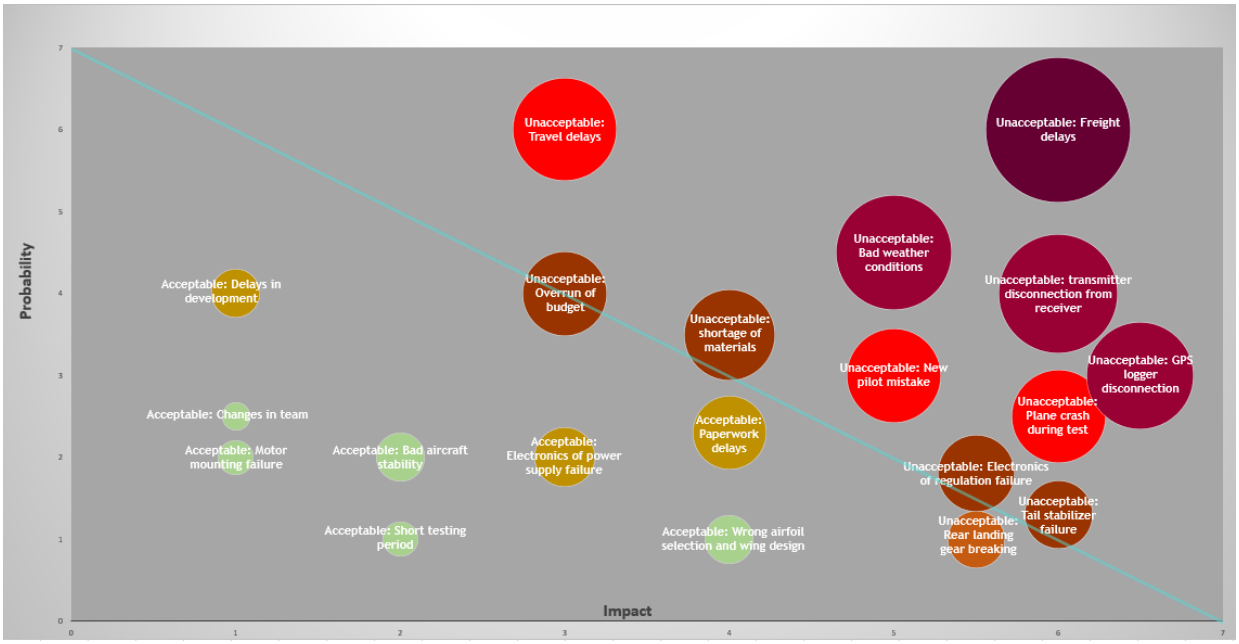

Figure 2 Risk bubble graph representation.

2.2. Software

To improve efficiency during the project, various computer programs were used. Utilizing this software allowed us to acquire more precise calculations results, make better decisions, and make communication easier and faster. Software choice was determined by its performance, ease of use, and team familiarity. All software and its use are shown in Table 1.

.

Table 1 Software used and its purpose.

Software		Purpose
Management	Clickup	Assigning tasks
	Zoom	Meetings organization, communication
	Google Drive	Files management
	ProjectLibre	Time management, project plan
CAD	AutoCAD	2D drawings
	SolidWorks	3D modelling
	Fusion 360	3D modelling and generative design
CFD, FEM	Ansys	Structural load analysis, flow analysis
	NX1980	Structural load analysis
Other	flow5	Aerodynamic configuration design
	xflr5	VLM analysis
	MS Excel	Charts and calculations

2.3. Work schedule

As mentioned above, the previous team, consisting of older team members, had to leave this project behind and hand it to the newer members. The older team managed to conceptualize and test the model using XFLR5 software, and then begin manufacturing and testing. Unfortunately, the pandemic struck and the competition had to be delayed. The table below shows how much time each team spent on each phase of the project. In early 2022, the newer team members took hold of the research and learned how to manufacture parts, then assembled the whole structure and started looking for imperfections in the structure to try and balance out. In parallel, the members were working on the technical report. In the beginning, the writing went tardily, but as time went on, things got back on track and the technical report was finished on time. Test flights began shortly after the end of the SAE Aero Design West competition. The fact that new pilots had to be trained increased the time required for testing.

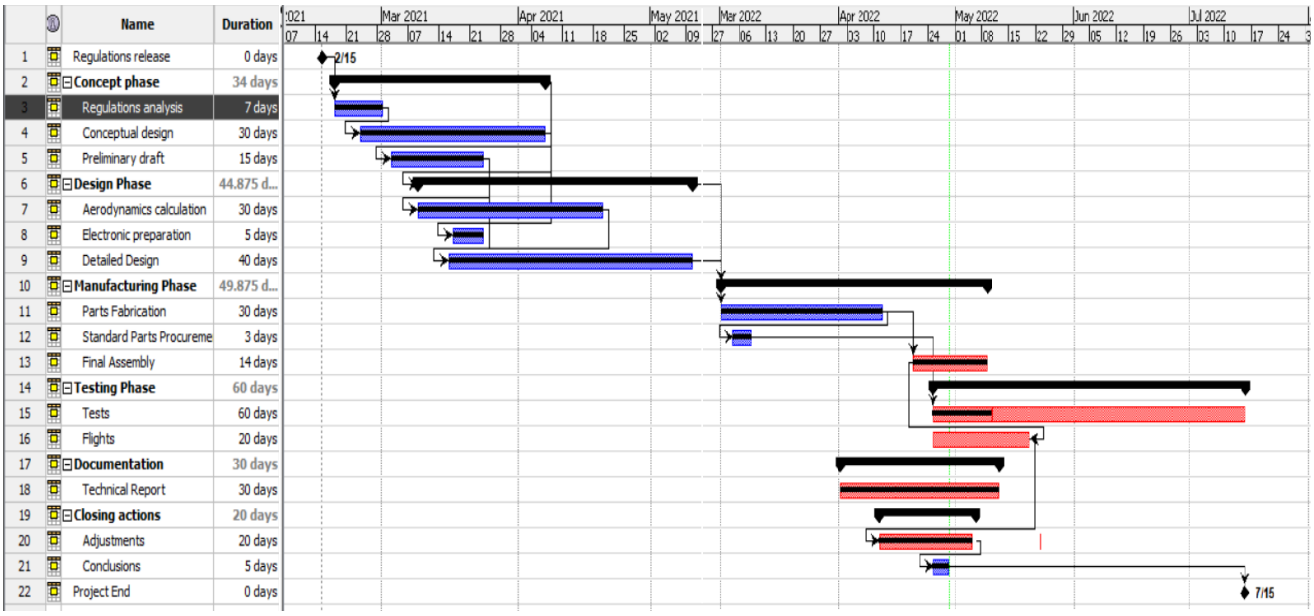

Figure 3 Table of work schedule.

2.4. Financial budget

Firstly, we participated in the competition for the distribution of funds at our university. Each participating team had to provide the relevant documentation, project timetable, distribution of funds, blueprints and staff allocation, as each team member was assigned according to their skills. All this information allowed the committee to subsidise our science club with the funds allocated to the ACC competition because they knew we were capable of doing it.

What is more, thanks to our previous achievements, we were chosen by the Dean's office as one of the five best strategic science clubs, which provided us with the necessary funding for this project. Thanks to our excellent results in other competitions, we have attracted many new sponsors from the industry, who have provided us with materials in the form of barter. Furthermore, we applied for grants from the Mechanical & Power Engineering Faculty and the Mechanical Faculty of Wroclaw University of Science and Technology. The final cost of each specific expense group can be seen in Table 2.

Table 2 Material costs.

Project expense	Value
Composite materials and chemicals	1 020 €
Wooden materials	310 €
Other, not enlisted materials (such as metal parts, etc.)	250 €
Services (such as milling, MJF 3d printing, etc.)	870 €
Electronics	930 €
Gas (needed to get to the airport for tests)	190 €
Build phase subtotal	3570 €
Members entry fee	1750 €
Car rental with fuel included	1050 €
Competition participation subtotal	2800 €
Project Total	6370 €

3. Mission, aircraft configuration, and dimensions

3.1. Scoring analysis

Due to the complex profile of this year's mission and scoring highly related to other teams' results. The team decided to calculate the most favourable variable, thus aircraft type, but quickly realized that too many variables were present. It was decided that an airframe with the best glide ratio possible and sustaining it at different speeds would be most beneficial for all scoring factors. To improve flight characteristics at low speeds e.g., at take-off and climb, wing mechanization in form of flaps was used.

3.2. Configuration selection

Maximum efficiency imposed the following features:

- good glide ratio – high wing aspect ratio and wing taper,
- best use of limited thrust – prop wash free of unnecessary elements,
- small frontal area – optimal cargo configuration.

As high aspect ratio and low drag wings are favourable, biplane and tandem configurations were rejected. To move the propeller away from other parts of the aircraft, the motor extends

on the CFRP tube in front of the aircraft. The cargo bay was moved down creating a parasol wing, to further remove propwash obstructions and improve airflow over the centre section of the wing. Carbon tube extends back creating tail boom, to which standard configuration empennage is attached. Other types of tail configuration were rejected, the as tail is located above the wing's downwash, making other, heavier, configurations unnecessary. The tricycle landing gear is used as it is easier to take off and offers better manoeuvrability.

Payload featured in this year's competition consists of blood bags filled with fake blood, which masses are 100g, 200g or 300g. Because at least one 300g bag must be carried, the team decided to use only these types of bags. Testing done by the team concluded, that 300g is close to the maximum capacity of the bag, thus its dimensions are mostly fixed, with only small shape changes possible. This resulted in considering the payload as a solid with a fixed shape and not as a liquid.

3.3. Aircraft dimensions

With aircraft dimensions partially fixed by a 1,5m rhombus shape, an optimal angle had to be found at which the aircraft would perform desirably. The most crucial factor was its longitudinal stability, as the static margin had to be greater than in other aircraft because of the payload which may shift CoG. The SM was set to 15%, contrary to the minimum of 5% used. Based on similar aircraft of this type, maximum horizontal stabilizer dimensions were determined. By changing the rhombus angle, the maximum wingspan at which SM of a minimum of 15% could be obtained was calculated using an MS Excel spreadsheet. The optimal angle was 112°, which resulted in a theoretical maximum wingspan of 2480mm, as shown in Figure 4.

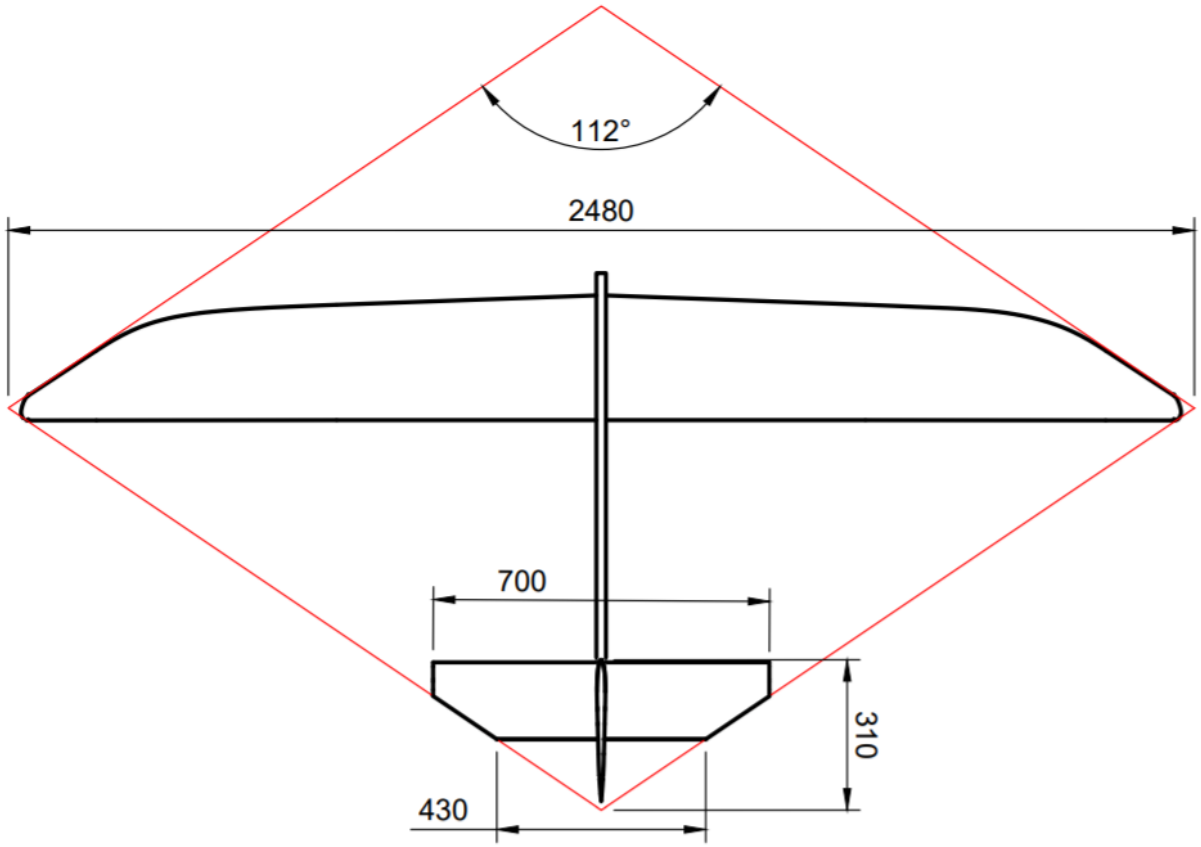

Figure 4 Aircraft draft inscribed in rhombus shape and resulting dimensions.

4. Aerodynamic design

4.1. Airfoil selection

As mentioned above, an airfoil with a high glide ratio and flat cl/cd polar curve had to be selected. To choose the best performing airfoil, the applicable Reynolds number had been calculated [2].

$$Re = \frac{V_{cr} \cdot MAC}{\nu} = \frac{12 \cdot 0{,}231}{14{,}55 \cdot 10^{-6}} = 198\,453$$

The lift necessary for the level flight was calculated from the lift force equation:

$$C_l = \frac{2W}{\rho \cdot S \cdot V_{cr}^2} = \frac{2 \cdot 9{,}81 \cdot 4{,}5}{1{,}225 \cdot 0{,}519 \cdot 12^2} = 0{,}96$$

Following these calculations, 4 airfoils were selected, shown in Figure 5and Table 3.

Table 3 Considered airfoils details

	Thickness, %	*At % of chord*	*Camber*	*At % of chord*
E216	*10,4%*	*26,2%*	*4,7%*	*59%*
MH32	*8,7%*	*30,2%*	*2,3%*	*45,7%*
A18	*7,3%*	*30%*	*3,9%*	*45%*
S1223	*12,1%*	*19,8%*	*8,1%*	*49%*

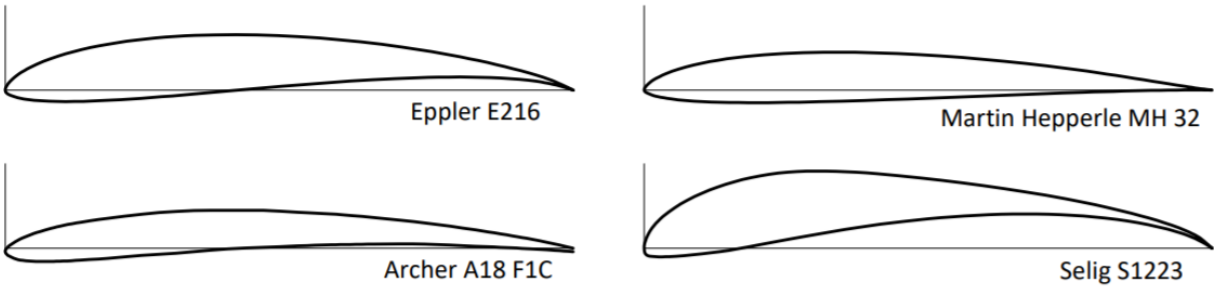

Figure 5 Considered airfoils shape.

Following airfoils were analysed using the XFlr5 program. Results are shown in Figure 6.

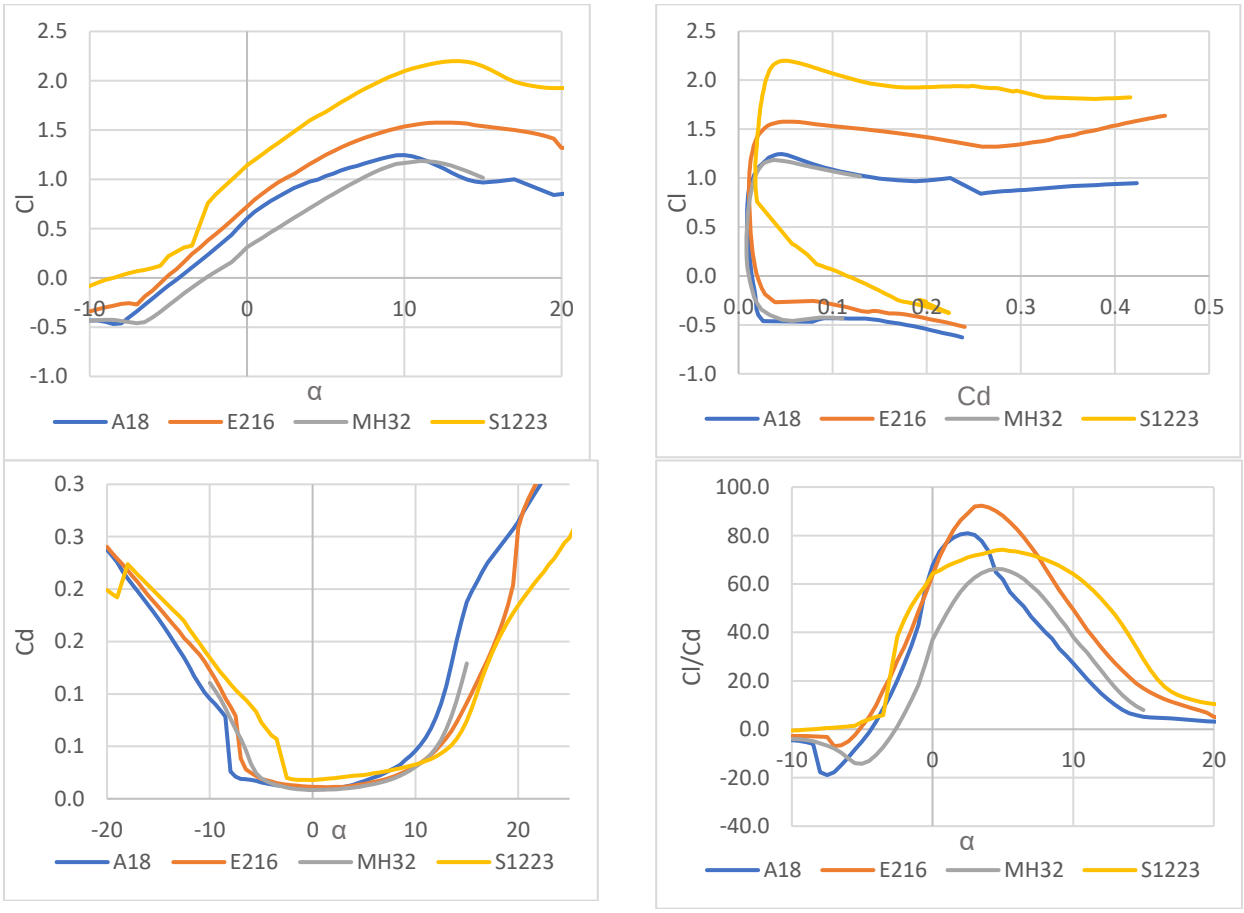

Figure 6 Airfoils polar diagrams.

Graphs show, that S21223 provides remarkably high lift, but at small α creates substantial drag, thus would not fit into the efficient-at-different-speeds design. MH32 was rejected as it doesn't provide enough lift margin. E216 was selected over A18 as it provides more lift at high α, and less drag at higher lift, which may be necessary during take-off and climb. Also, A18's very thin profile could lead to mechanical challenges during the wing construction process.

4.2. Flap chord selection

Effective wing mechanization was described as an important feature. For flaps to be a viable solution, lift must be increased by a noticeable margin and increased drag can't prevent aircraft from slowing down. As all tested flap chords performed well, one with the highest glide ratio, which occurred with a 30% MAC flap, was selected as best for the climb (Figure 7).

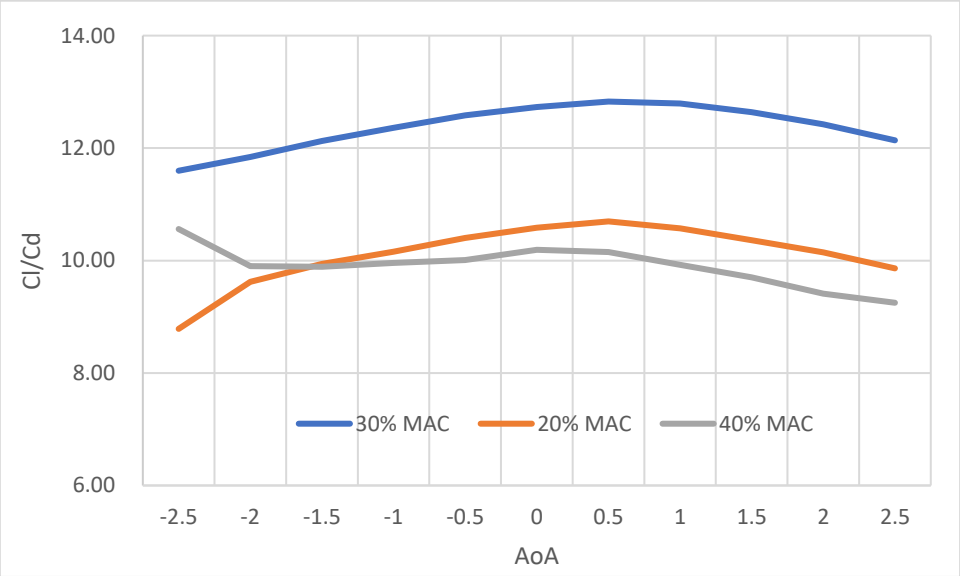

Figure 7 Drag to lift coefficient for different % chord flaps.

4.3. Wing geometry

With established lift coefficient and lift force, the maximum take-off weight was calculated. Stall speed was established with lift coefficient decreased by 10% as an aircraft should not exceed the maximum angle of attack at a low altitude as the one occurring during the competition. The maximum aerodynamic load of the wing was calculated for aircraft controllability analysis [1].

Table 4 Final wing parameters

Wing Span	2,4m
Wing Aera	0,521m^2
Aspect Ratio	11
Taper Ratio	0,2
MAC	0,229m
Dihedral Angle	3

$$L = \frac{1}{2}\rho v^2 S C l_{MAX} = 0{,}533 m^2$$

$$Cl_{MAX} = 1{,}35$$

$$v = 10\,{}^{m}/_{s}$$

To fit inside rhombus shape, wingtips are tapered and have their tips rounded off for safety and strength. A 3° dihedral was added to the wingtips to increase roll stability (Table 4, Figure 8).

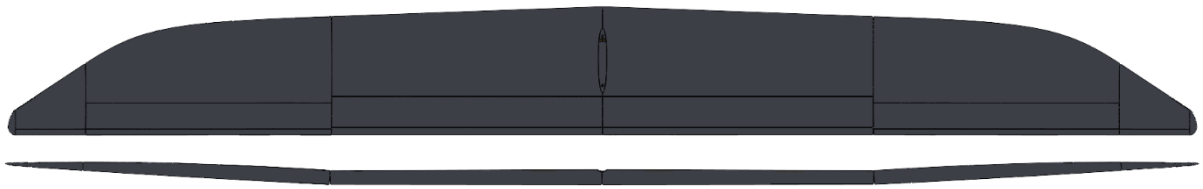

Figure 8 Finished wing design.

4.4. Fuselage design

Mission profile requires flying at various speeds during a single flight, thus single AoA for a flight cannot be determined. A rather long shape of the fuselage could drastically increase drag and generate unwanted lift/downforce if subjected to a suboptimal (different than 0) angle of airflow. To mitigate this problem, it was decided to design the fuselage in an aerodynamic shape such as an oval. After designing several prototypes, it became clear that oblong blood bags cannot be fitted inside an oval fuselage with minimal free space. Also, the fuselage which could fit the payload inside would be too high, making the aircraft exceed 50cm in height, and its frontal area would be larger than the rectangle one.

The idea was dropped, and a rectangular fuselage with a fairing at either end was designed. After test flights of the prototype, its incidence was set to be 0 degrees during circling according to tested AoA, as during the climb it can contribute to total lift generated. To allow flight with varying cargo amounts, it is located directly below CG, introducing no shifts in stability margin.

4.5. Aircraft stability

Our team has carried out the dynamic and static analysis in XFLR5 software (Figure 9). The centre of gravity is at 30,5% of MAC. To ensure safety, our team decided to provide a higher than usual static margin for our aircraft, as cargo may shift its position during the climb. The neutral stability is located at 53,5% of MAC. It means that SM is 23%. After locating the CG and adding all masses of each component, we checked static and dynamic stability.

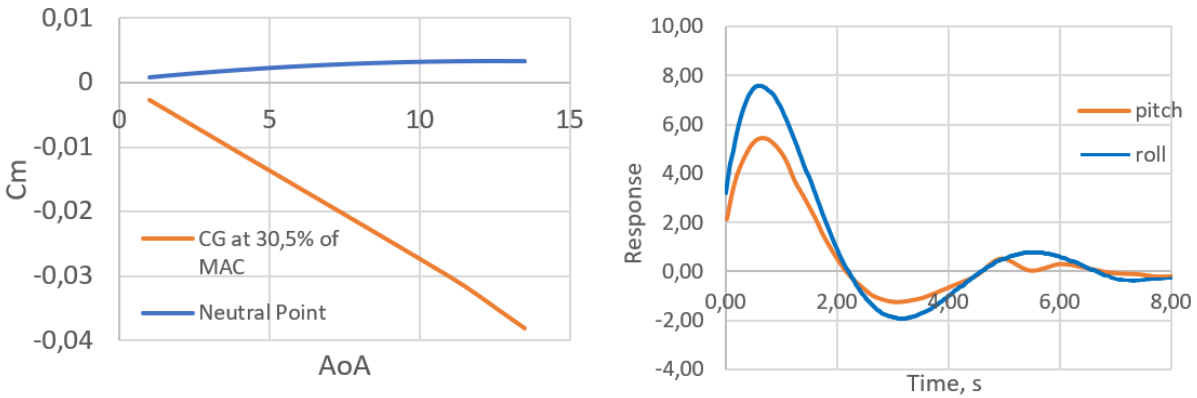

Figure 9 Static and dynamic stability.

The oscillations tend to decay over time- which means the aircraft is stable [4].

High pitch stability is mainly provided by the low CG position, thanks to the cargo located substantially below the wing.

5. Aircraft performance

5.1. Take-off distance

Considering that the take-off distance is 60 meters long, it was necessary to calculate how much cargo can be loaded on the plane, so that it would still be able to take-off with its payload and meet the restriction. We have also taken into account that the air density could vary with

weather conditions which would affect the take-off distance therefore the maximum load weight is a little less than it could theoretically be [6].

Table 5 Take–off distance.

Weight Force (Plane + Payload)	44,145 N
Thrust	13,73 N
Take off velocity(V)	11,78 m/s
The lift coefficient (at take-off)	1
Take off distance(L)	**35 m**

The take-off velocity was calculated using the following equation:

$$V = \sqrt{\frac{W}{\frac{1}{2}\rho S C_{lTO}}}$$

Whereas the lift force at take-off was calculated using this one:

$$L = \frac{W}{g\rho S\left[C_{lTO}\left(\frac{T}{Q} - \frac{\mu}{2}\right) - \frac{C_x}{2}\right]}$$

Following values are:

$$V = \sqrt{\frac{44{,}145}{\frac{1}{2}\cdot 1{,}225 \cdot 0{,}52 \cdot 1}} = 11{,}773$$

$$L = \frac{44{,}145}{9{,}81 \cdot 1{,}225 \cdot 0{,}52\left[1\left(\frac{13{,}734}{44{,}145} - \frac{0{,}1}{2}\right) - \frac{0{,}03}{2}\right]} = 35$$

To estimate the take-off distance, we used the following equation and graph (Figure10).

$$TOP = \frac{p}{\sigma C_{lTO}\frac{T}{MTOW}} = \frac{\frac{4{,}5}{0{,}52}}{1\cdot 1{,}2\cdot\frac{13{,}734}{61{,}803}} = 139{,}08$$

$$p = \frac{W}{S} \quad P_{lTO} = W \qquad 1C_{lTO} = \left(\frac{V_{min}}{V_{TO}}\right)^2 C_{lMAX}$$

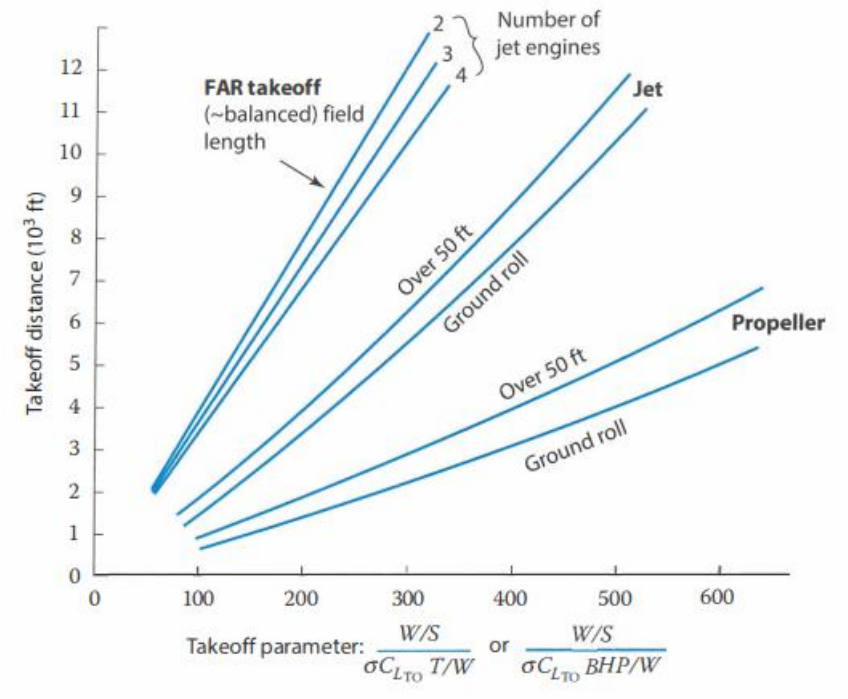

Figure 10 – Take-off distance estimation.[7]

The minimum velocity required for levelled flight at 0 m is 11.78 m/s which is achieved at 35 meters of full throttle.

5.2. Climb-out performance

The climbing time is 60 seconds for the plane to ascend as high as possible during this time. The climbing performance of the plane depends on many factors. By calculating the rate of climb that results from the product of the minimum required velocity for take-off and the angle of climb, it is determined what height the plane will be at after 60 seconds and after what time it will reach the level of 100 meters.

Table 6 Climb–out performance

Rate of climb (R/C)	1,8 m/s
Lift force (Pz)	56,87 N
Drag force (Px)	1,32 N
Angle of ascent	9°
Time up to 100 meters	55s
Height after 60 seconds	**110 m**

The equations used for the calculations [6]:

$$\frac{R}{C} = V\sin(\gamma) \qquad P_z = C_{lF}\frac{\rho V^2}{2}S \qquad P_x = C_x\frac{\rho V^2}{2}S$$

$$p_c = \left(\frac{T}{MTOW} - G\right) + \frac{\sqrt{\left(\frac{T}{MTOW} - G\right)^2 - 4C_{d0}\frac{1}{\pi\lambda e}}}{\frac{2g}{q_c\pi\lambda e}} + 2$$

The following values of those are:

$$\frac{R}{C} = 11{,}773 \cdot \sin(18°) = 3{,}665$$

$$P_z = 0{,}28\frac{1{,}225 \cdot 11{,}773^2}{2} \cdot 0{,}52 = 56{,}87$$

$$P_x = 0{,}03\frac{1{,}225 \cdot 11{,}773^2}{2} \cdot 0{,}52 = 1{,}324$$

$$p_c = \left(\frac{13{,}73}{44{,}145} - 0{,}138\right) + \frac{\sqrt{\left(\frac{13{,}73}{44{,}145} - 0{,}138\right)^2 - 4*0{,}03*\frac{1}{\pi*e*11{,}06}}}{\frac{2*9{,}81}{103{,}5125*\pi*e*11{,}06}} = 17{,}9915$$

$$G = \frac{w}{V_t}$$

Following values are:

$V_t = 13\ m/s$ $\quad G = \frac{1{,}8\ m/s}{13\ m/s} = 0{,}138$ $\qquad qw = \frac{1{,}225*169}{2} = 103{,}5125$

The condition is fulfilled, the lift surface load during climbing is bigger than the assumed lift surface load during levelled flight. Climbing is safe and meets desired value.

V - take off velocity; R/C - rate of climb; Pz - lift force; Px – drag force;

C_{lF} - Lift coefficient (during the flight); ρ - air density; S - lifting surface; Cx - drag coefficient;

C_{lTO} - Lift coefficient (at take-off);

6. Structural design

This part presents design solutions used in each subassembly of the aircraft: engine nacelle, tail boom with empennage, wing, cargo bay with front and rear undercarriage.

6.1. Engine nacelle

The electric motor is connected to the tail boom by a monocoque construction carbon fibre nacelle. A 3d printed motor housing is used to minimize drag while providing necessary cooling during flight. Two birch plywood bulkheads provide support for the motor and tail boom tube at either end. Nacelle also houses the motor battery, ESC and main receiver.

Figure 10 Engine pod (note safety nut installed).

6.2. Tail assembly

To decrease empennage weight, both stabilizers are constructed with balsa wood with minimal use of birch plywood only in connection points. The main spar uses carbon fibre flat bars as a light alternative to pine. All surfaces are covered with OraCover OraLight covering foil providing a smooth surface and increased stiffness while keeping weight to the minimum. Both stabilizers are mounted to a carbon fibre tail boom by 2 screws and an aerodynamic 3d printed adaptor. During construction, 3d printed jigs (Figure 9) were used to position all elements and simplify the construction process[3].

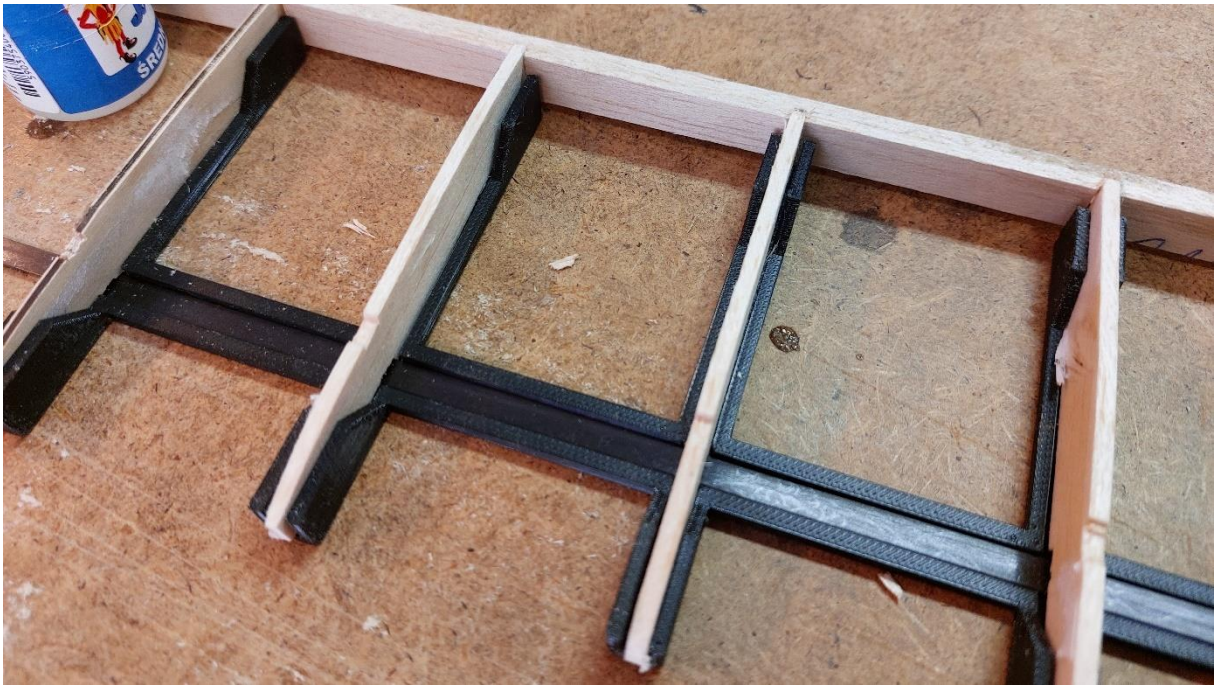

Figure 11 Stabilizer construction process using 3d printed jig.

6.3. Wing

The wing is a stressed skin type of construction composed of a carbon fibre composite sandwich structure. The laminate was chosen over wooden construction, as it is easier to manufacture while providing greater quality of the air foil's shape. As the moulds for the wing were already made, we didn't have to worry about the overall higher cost compared to wooden construction. Wing shell is composed of two layers of Aspro spread tow carbon fabric, followed by ROHACELL structural foam and a third layer of carbon. Application of core material increases product thickness; thus, stiffness is increased with little weight added. A minimal amount of internal structure is used, as tests are done by the team concluded that resin used to connect them to the wing's shell heavily contributes to the overall weight. The exact arrangement of internal structures can be seen in the Figure below (*Figure 12*).

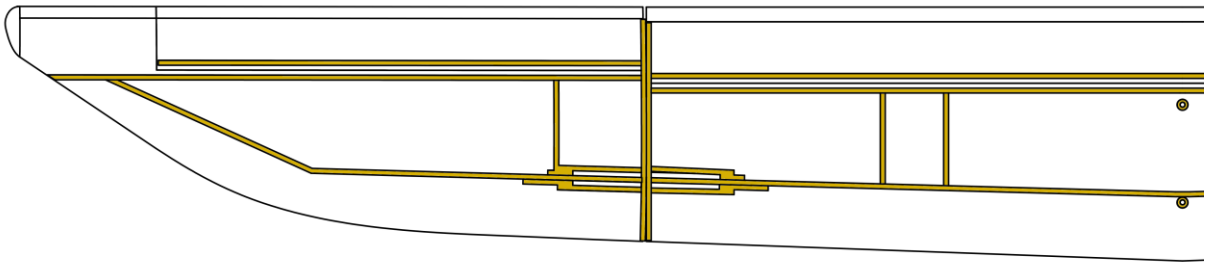

Figure 12 Arrangement of internal structures inside the wing.

The only ribs that were necessary are the ones that are located near the servos, as the rest of the shell presents satisfactory stiffens. In wingtips, the spar extends beyond what is necessary during flight, to prevent buckling of wing skin during the static load test. Control surfaces hinge is created by laminating a strip of peel ply between carbon fibre layers creating a secure and bendable connection. To comply with the transportation box requirement, the wing was divided into a centre section and two wingtips. A composite bayonet connects two parts and sets the correct angle in between them, as wingtips provide dihedral for the wing. Two cavities in the centre section are made to provide space for an automated measuring device and RC electronics with an RC battery. To improve tail boom positioning, a circular slot on top of the wing is created.

6.4. Fuselage

Depicted in the aerodynamics section, the fuselage features a rectangle cross-section, with corners rounded off to keep blood bags in one, tight package. Blood bags are located in 2 columns containing 3 bags each placed flat, resulting in 6 bags/1900g total. This configuration was chosen as in the 3x2 configuration the nosecone would be too close to the propeller. A wooden cargo bay prototype was made to determine the dimensions at which bags would fit snugly inside, while still being able to be taken out. The final dimensions were set as 120x110mm, with a 30mm edge radius. The fuselage attaches to the underside of the wing with a single pylon and two M4 screws. A single plywood frame located in the nosecone provides support for the front landing gear mount and its servo. Main landing gear, located at the back is directly attached to the fuselage without the assistance of a frame, as cargo is accessed from the back. The location of such cargo door was chosen as it is the least weakening to fuselage structure and allows to remove all bags in a single pull with the help of a plastic foil wrapped around them.

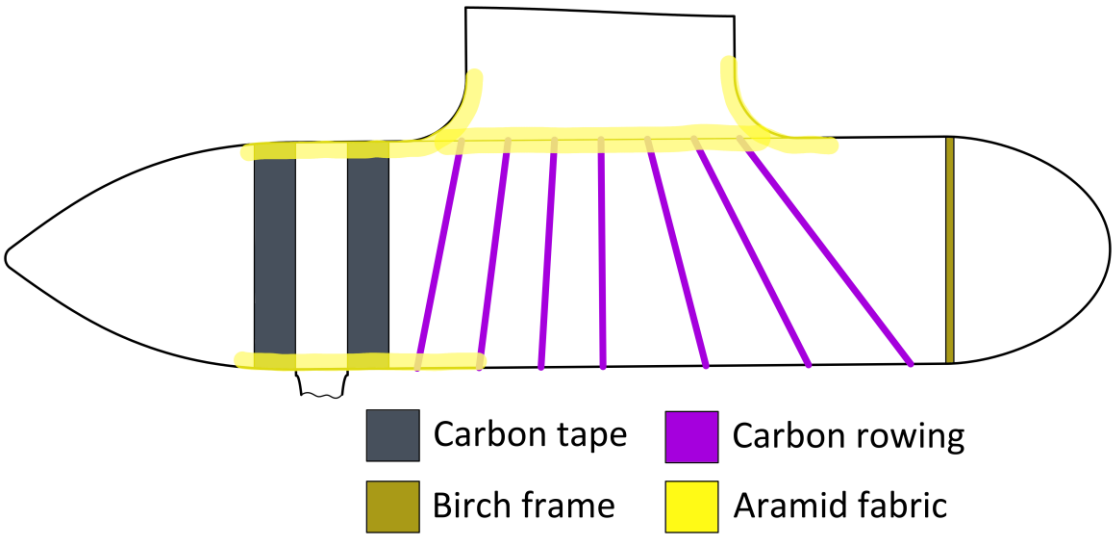

Figure 13 Fuselage internal structure.

The fuselage is made using a CFRP sandwich. In places where significant point loads occur (e.g., main landing gear, pylon) aramid fabric is used (Figure 9), to spread out cumulated forces and increase impact strength [1]. Carbon roving strands are run radially from the pylon to increase shell stiffness and carry distributed loads created by payload into screws connecting the fuselage to the wing. To replace the rear frame, unidirectional carbon tape is added to replace core material to keep inside dimensions uniform.

6.5. Front landing gear

The uneven surface of the grass runway had a substantial impact when designing front landing gear. To dampen vibrations, using our experience, the team selected telescopic landing gear design as being simple to build and pairing well with unretractable landing gear. Trailing link design was also considered but was rejected as it may catch onto the grass and cause a turnover resulting in mission failure. To decrease aerodynamic drag, a connection point with the airplane is located inside the fuselage nosecone. We decided to manufacture this part using MJF 3d printing technology, thanks to one of the sponsors who gave us a coupon for their services. Given the required parameters, a generative design process was run to create a lightweight part, which then was printed (Figure 14.).

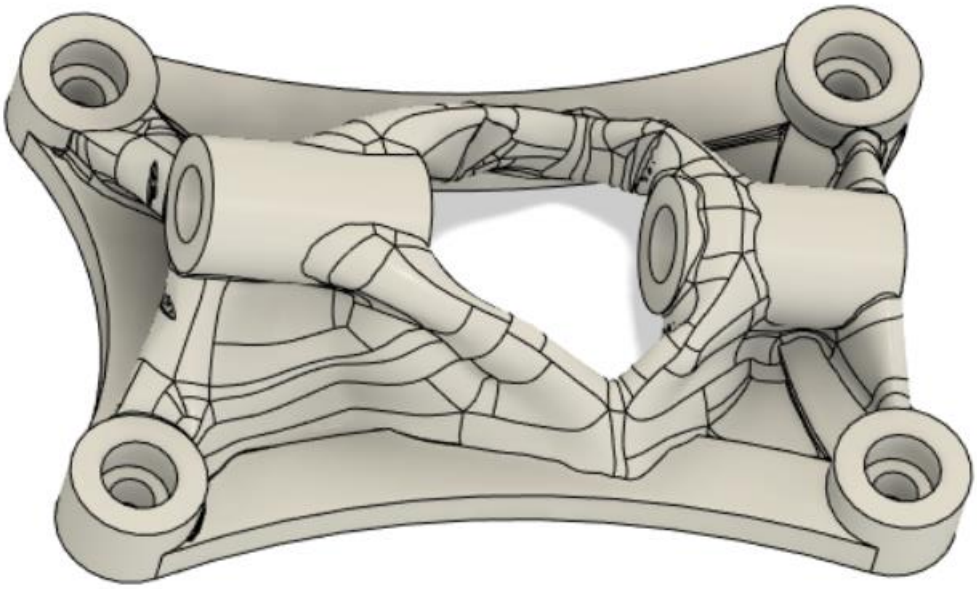

Figure 14 Generatively designed front landing gear part.

6.6. Main landing gear

The main landing gear was designed for easy production and to be quickly replaced in case of failure. To form the basic shape of this part, an exponential function was used as its curvature allows for a smooth transition between level and horizontal, thus no stress hotspots are created. Parts were manufactured by sandwiching Herex – foamed PVC core material, with layers of carbon fibre and aramid fabric providing strength and carbon roving strands providing stiffness (Figure 15). The amount of each material was selected experimentally until the landing gear presented satisfactory strength and stiffness compared to its weight [1].

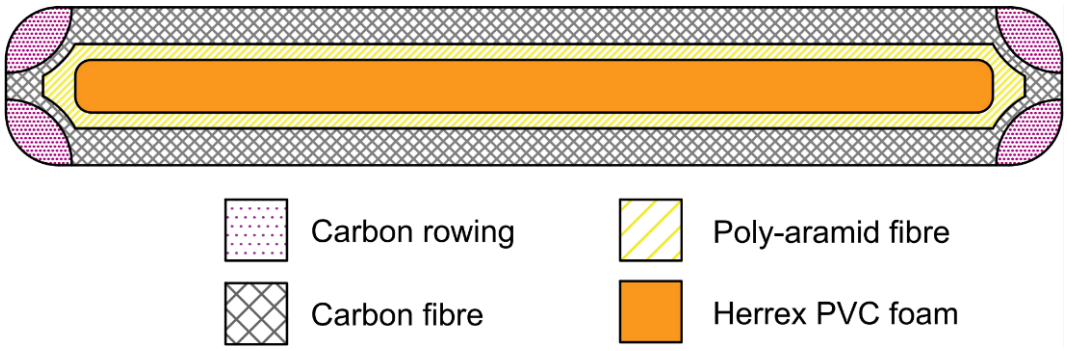

Figure 15 Landing gear cross-section

7. Battery testing

With the propeller and motor imposed by the rules, the only component having a significant impact on thrust is the battery. Only 3S LiPo batteries were considered, as these provide the

highest voltage, thus spinning the motor faster. To determine optimal battery size, static tests followed by testing flights have been performed. Results showed that both 2650mAh and 2200mAh batteries have enough capacity to safely perform flight task while having a reserve for 3 landing attempts (Figure 16).

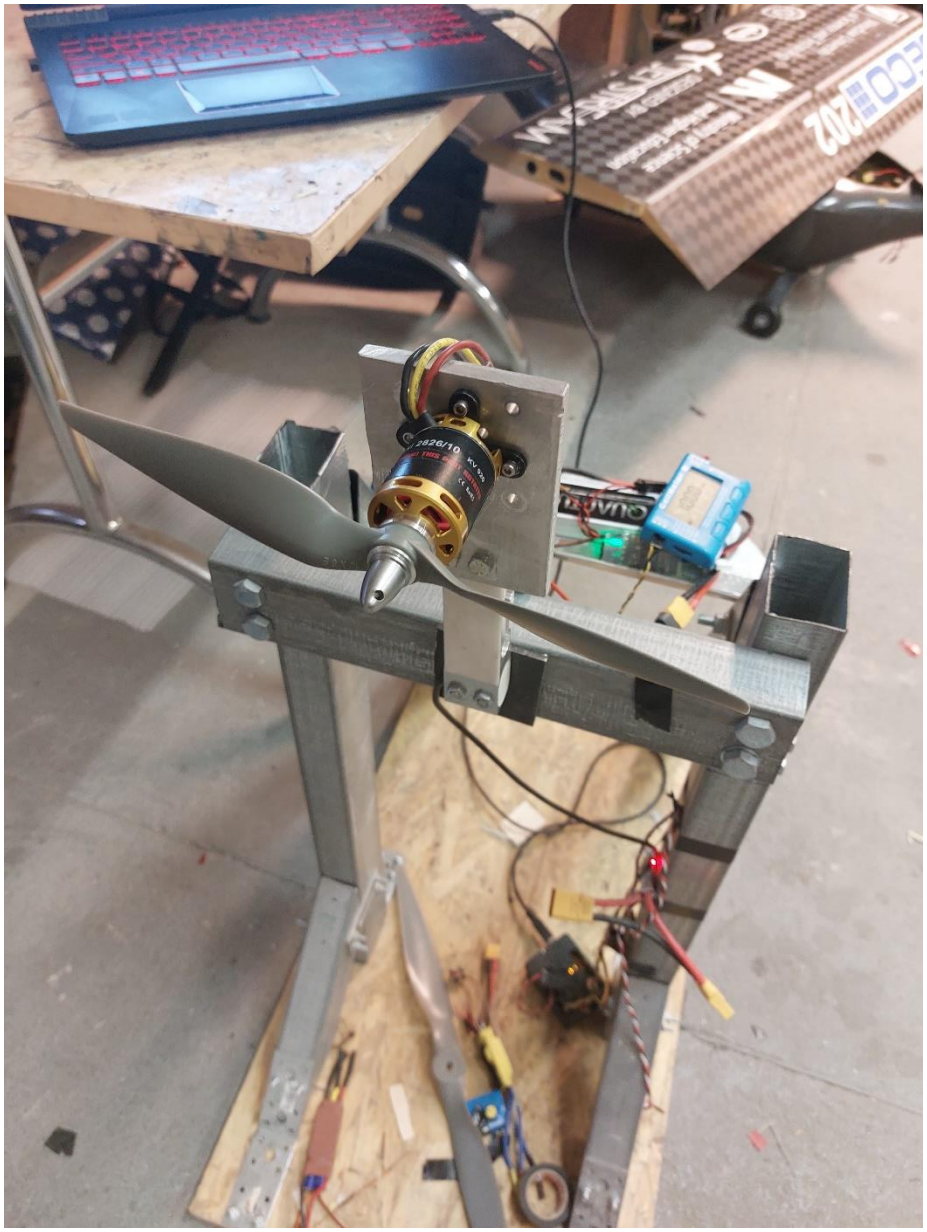

Figure 16 Static engine test stand.

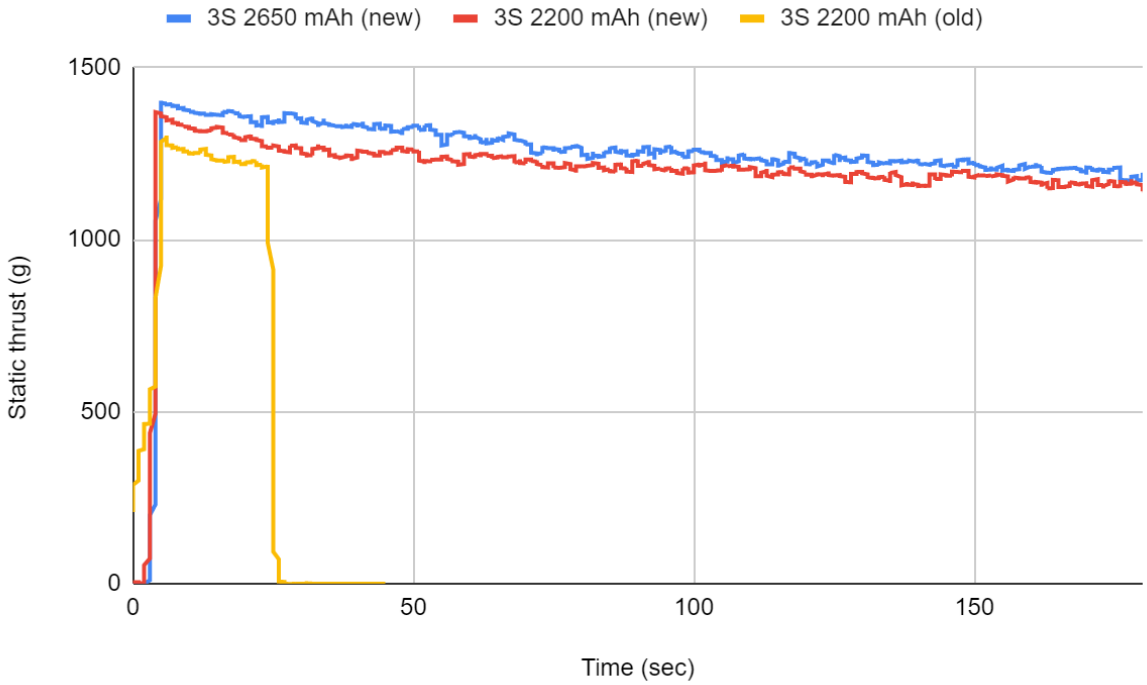

Figure 17 Static motor results.

A 3S 2600 battery was chosen as it provided much more thrust during the first 60 seconds of the test, which in flight covers the whole climb phase of the task. Larger batteries were not tested, as power gain would be minimal and not offset increased weight. Also, an old battery was tested to compare its performance with a new one, resulting in a power loss of as much as 12%. To provide the best performance during the competition, a set of new batteries were bought.

8. Electrical and electronic setup

The electrical system was designed to provide ease of aircraft assembly and operation and is divided into power and aircraft control sections. The power section is housed in the engine nacelle and consists of a motor, ESC, battery monitor and the 3S 2650 mAh battery. Locating all the components in one place uses minimal wire length reducing power losses. A battery monitor is installed to indicate to the pilot how much power he has left to help him with estimating maximum power during the descent.

The aircraft control section is located in a cavity in the right portion of the centre wing (Figure 15), to counterbalance the automated measuring equipment's weight located on the opposite

side. As required, 2S 800 mAh LiPo along BEC is used to power all devices onboard. Common power and neutral wires are used to power servo motors onboard to conserve mass. Two RC receivers located at either end of the carbon tube are used to reduce the risk of carbon body shielding radio waves.

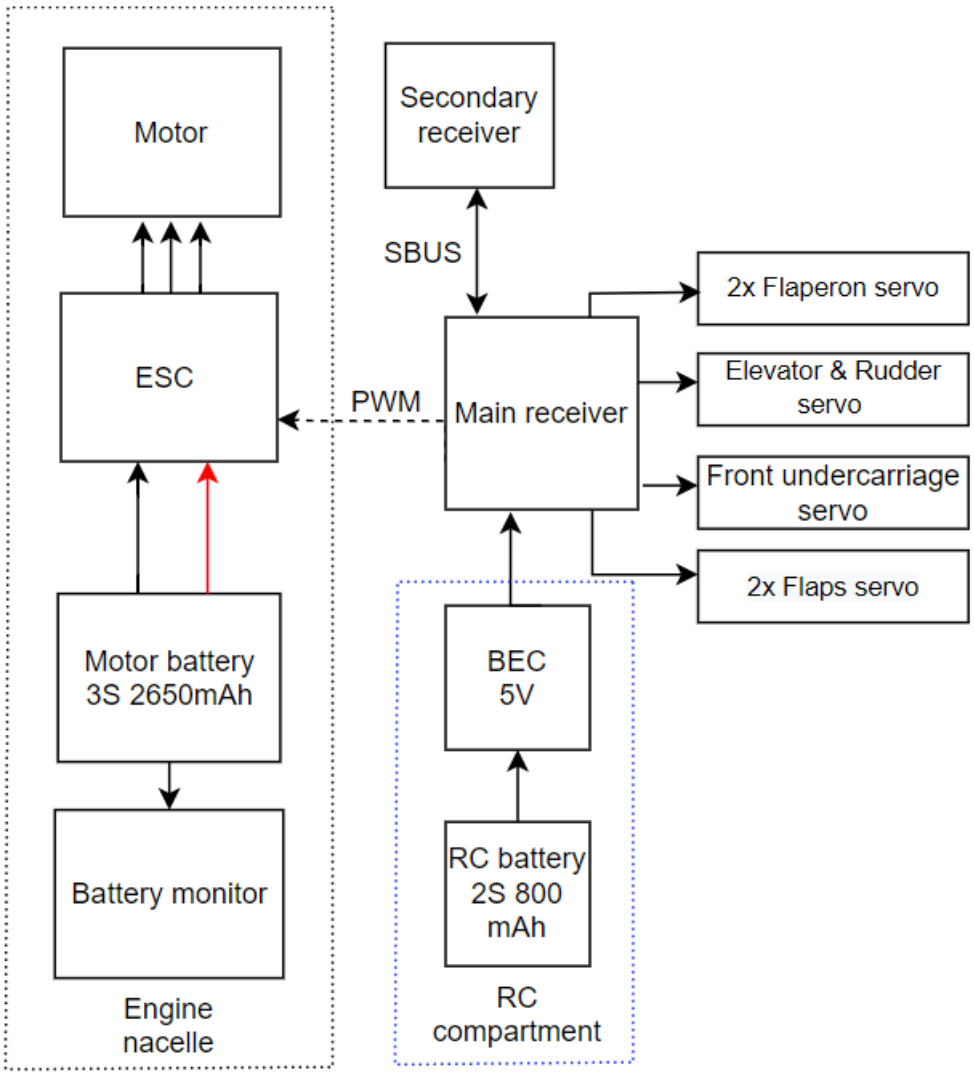

Figure 18 Electrical setup.

9. Control surfaces sizing and servo selection

To obtain short take-off the team decided to construct flaps along the whole wingspan, with flaperons at the wingtips. Using xflr5, it was determined that 30% of mean chord flaps provide the best results with the used airfoil. Flaperons don't extend to the end of the wingtips for construction durability.

Based on literature studies, similar aircraft types and team experience elevator and rudder sizes were selected as 35% and 40% respectively. These sizes are larger than normal as the possibility of small cargo shift and high crosswinds were taken into consideration.

Torques acting on servos were calculated using the empirical equation shown below:

$$M = \left(-0{,}235 \cdot \left(\frac{l_s}{L_s} - 0{,}2\right) + 0{,}164\right) \cdot \frac{a}{20} \cdot S_a \cdot l_s \cdot 0{,}6 \cdot \left(\frac{V_{max}}{3{,}6}\right)^2$$

where:

l_s – mean control surface cord [m]; L_s – mean geometric wing cord [m]; a – maximum surface deflection [°]; S_a– control surface aera [m^2]; V_{max} – maximum velocity [km/h] ; M – control surfaces moment.

An MS Excel spreadsheet was created (Figure 16) to calculate maximum torque acting on flaps and flaperons, as their maximum deflection angle does not correlate with maximum speed.

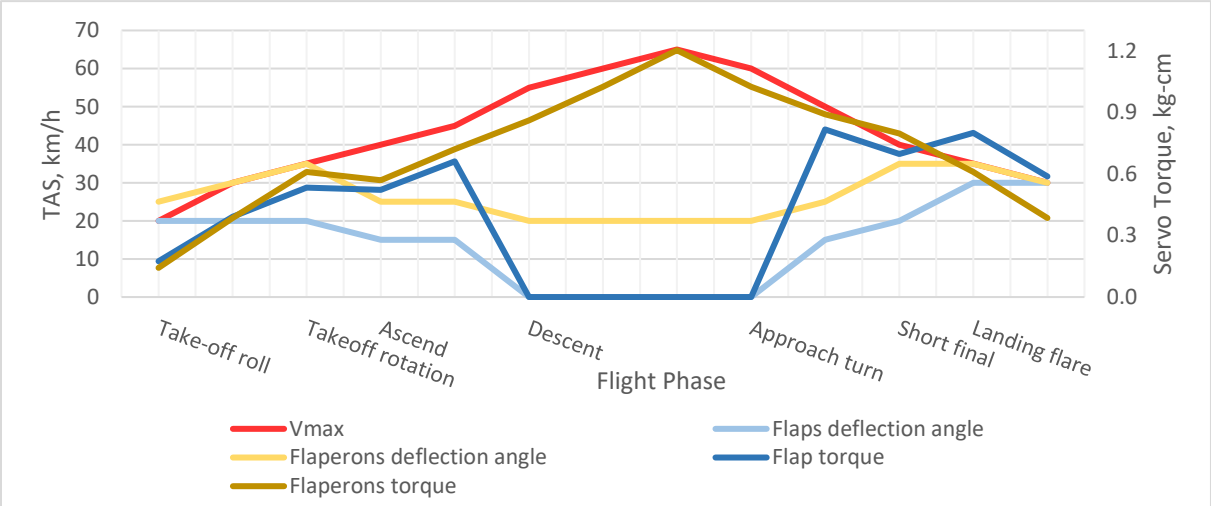

Figure 19 Servo torque relative to TAS and deflection angle.

Table 7 Maximum torques and selected servo motors.

Control Surface	Surface Torque kg-cm	Servo Type	Servo Torque kg-cm
Flap	0,82	Savox SH-0255MG	3,4
Flaperon	1,20	KST DS. 125	5,9
Elevator	1,03	Savox SH-0255MG	3,9
Rudder	0,70	Dualsky DS169	2,3

Maximum torque created by each control surface and the selected servos motors along with the rated torque (Table 7). It was decided to use a safety margin of at least 3, because of our

last experience during the SAE Aero Design competition, when the selection of too small servo caused a total loss of 3 aircraft models. The space inside wingtips was too small to fit standard sized servo inside, thus KSD DS 125 servo is used.

10. Test flights

When the message about the 2021 competition postponement was posted, the team had already milled out necessary moulds except the fuselage one. It was decided to create a mock-up fuselage, test the aircraft design and create a new fuselage tailored to real-life data. Flights concluded, that 2,5kg can be lifted without problems, but 2kg shows superior performance during the descent part of the mission. As design philosophy demanded efficiency, a 2kg option was selected and an appropriate fuselage was designed. New cargo bay design allowed to reduce its mass by 30%.

Figure 20 Aricraft during test flights.

11.Payload Prediction

The payload prediction function was derived from the lift equation. MS Excel spreadsheet was used to calculate and plot (Figure 20) the correct payload at various air densities, based on data obtained during test flights of the prototype.

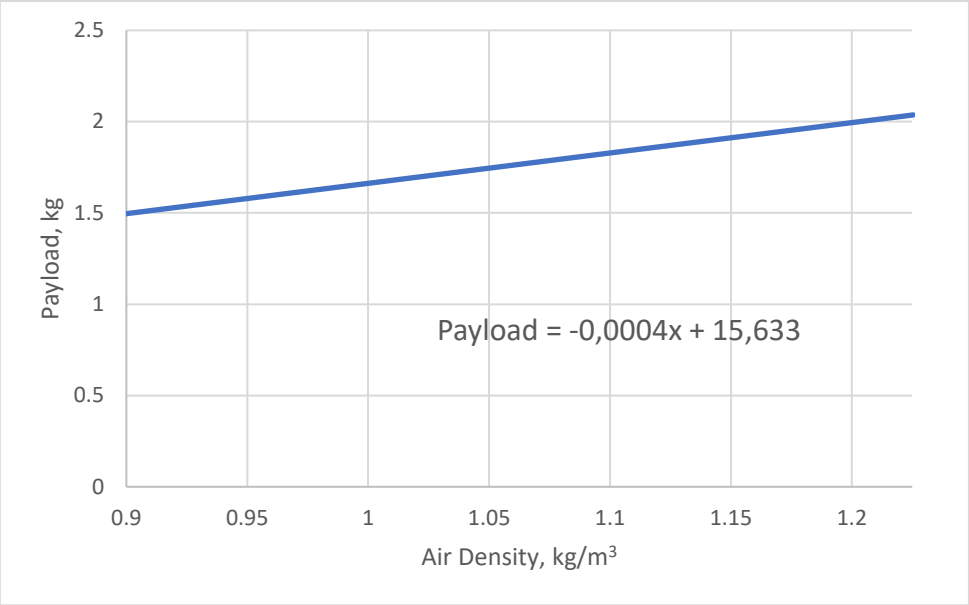

Figure 21 Payload Prediction Curve.

12. Outlook

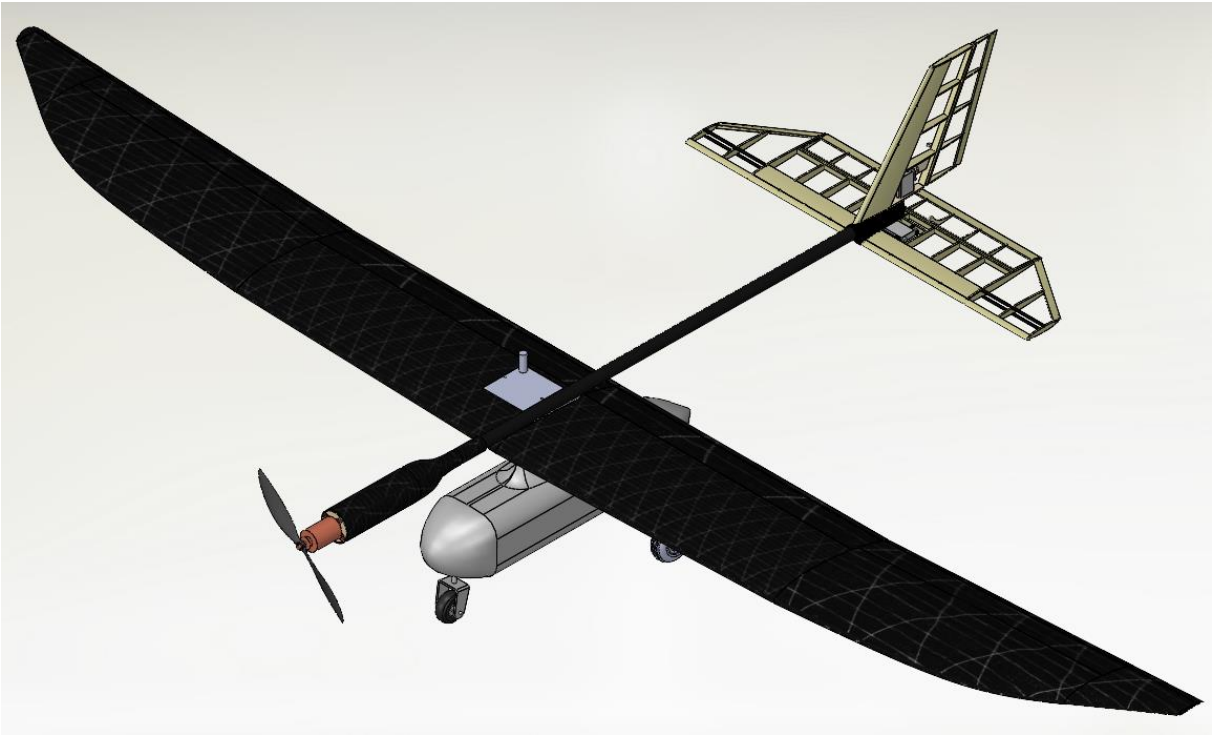

Figure 22 Outlook.

13. Conclusions

Because of the quickly approaching report submission deadline, we haven't managed to do a lot of test flights. Moreover, our team doesn't have a proper fuselage mould yet due to a long waitlist. However, while our team waits for the moulds, we are using a fuselage from a

previous Air Cargo Challenge competition and building a prototype to increase the number of test flights and further develop our understanding of the project.

After obtaining an up-to-date fuselage, it will be tested to check how it flies and behaves in the air. Such empirical studies should allow for further optimization of the aircraft and reductions in weight by determining where additional reinforcements are needed or the opposite – where strength could be exchanged for some weight savings. Further care will be taken to ensure that the loading and unloading process is quick, reliable, repeatable and does not result in damage to either the cargo or the fuselage. Another important consideration would be making sure that the plane is reasonably easy to fly for the pilot, as the team's performance is highly dependent on it.

14.Table of Figures

15.Table of Tables

Table of References

- [1] “Budowa samolotu obciążenia” - Witold Błażewicz
- [2] “Podstawy aerodynamiki i lotów” - W. Nowakowski, A Ablamowicz
- [3] Cichosz E, Trościanko S (1972) Poradnik do projektowania samolotów – część 1. Wydawnictwa Komunikacji i Łączności WKŁ
- [4] Roskam J (1985) Airplane Design. Design, Analysis and Research Corporation
- [5] Kundu A (2010) Aircraft Design. Cambridge University
- [6] Władysław Fiszdon, Mechanika lotu cz.1
- [7] Danie P. Raymer (2010) Aircraft Design: A Conceptual Approach

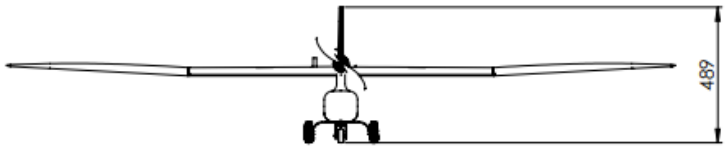

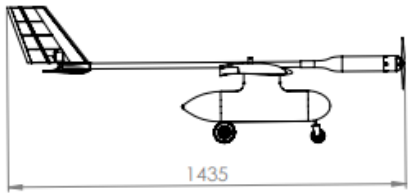

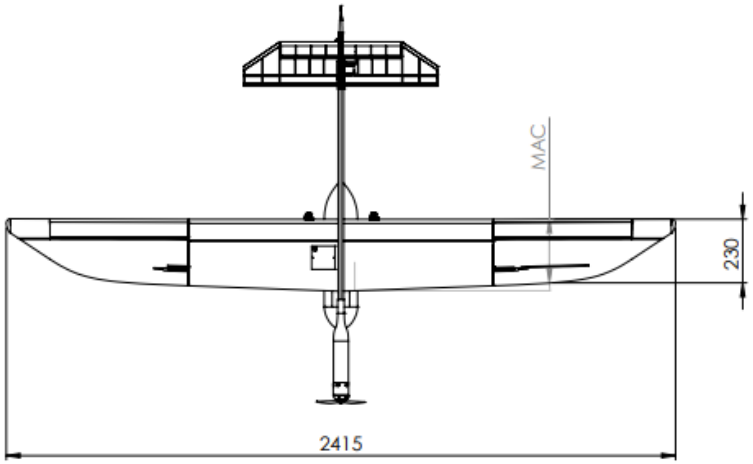

Aircraft data table	
Wingspan	2415 m
Lenght	1435 mm
Height	489 mm
Wing airfoil	Eppler 216
Wing area	0,52 m2
Vertical stabilizer area	0,03 m2
Horizontal stabilizer area	0,1 m2
Empty weight	2,5 kg
Loaded Weight	4,5 kg
Motor battery capacity	2650mAh 3S1P 11,1V 45C/90C
Electronics battery capacity	800mAh 2S1P 7,4V 30C/60C
Engine make & model	AXI 2826/10 GOLD LINE V2
Propeller	APC-E 10x6E
Flaperon servo	KST DS125MG
Flaps & elevetor servo	SH-0255MG
Rudder servo	DUALSKY DS169 DIGITAL
Front wheel servo	HiTEC HS-645MG

JETSTREAM

Wroclaw University of Science and Technology

	NAME	DATE
DESIGNED	Mateusz Kuchanski	20.04.2022
DRAWN	Jacek Napora	20.04.2022
CHECKED		

Unmanned Aerial Vechicle for transport of medical emergency goods

SIZE: A3 | SCALE: 1:15 | SHEET 1 OF 4 | TEAM NAME: **JETSTREAM** | TEAM NO.: **21**

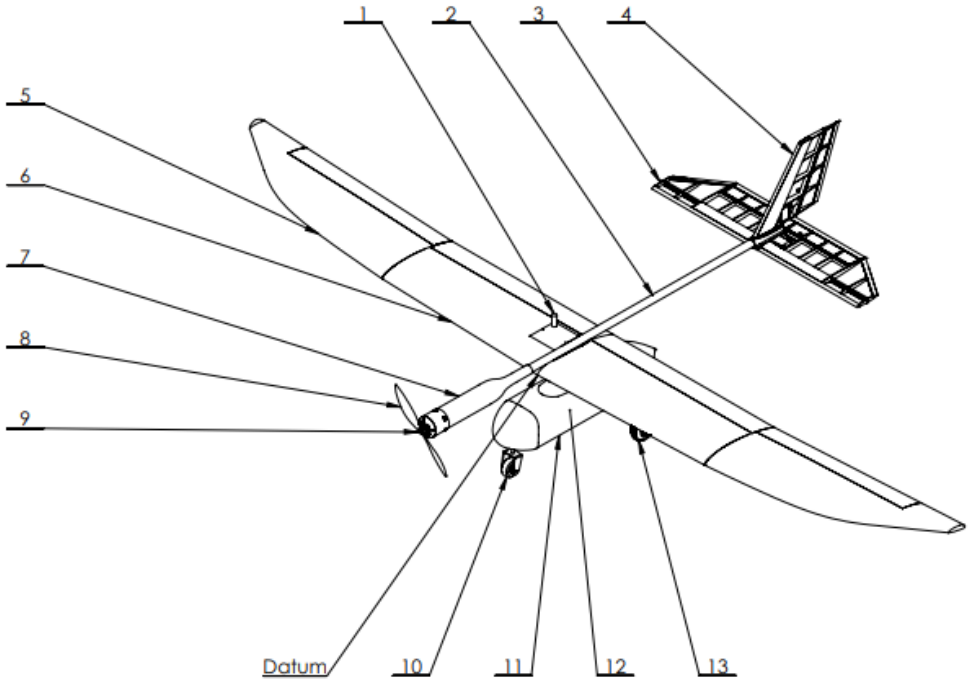

Table of parts	
1	Automated Mesuring Equipment
2	Fuselage pipe
3	Horizontal stabilizer
4	Vertical stabilizer
5	Outer wing
6	Center wing
7	Batteries
8	Propeller
9	Electric motor
10	Front udercarriage
11	Cargobay
12	Payload
13	Rear undercarriage

Annotation:
- Datum is located on a center of a leading edge

JETSTREAM

Wroclaw University of Science and Technology

	NAME	DATE
DESIGNED	Mateusz Kuchanski	20.04.2022
DRAWN	Jacek Napora	30.04.2022
CHECKED		

Unmanned Aerial Vechicle for transport of medical emergency goods

SIZE: A3 | SCALE: 1:10 | SHEET 2 OF 4 | TEAM NAME: **JETSTREAM** | TEAM NO.: **21**

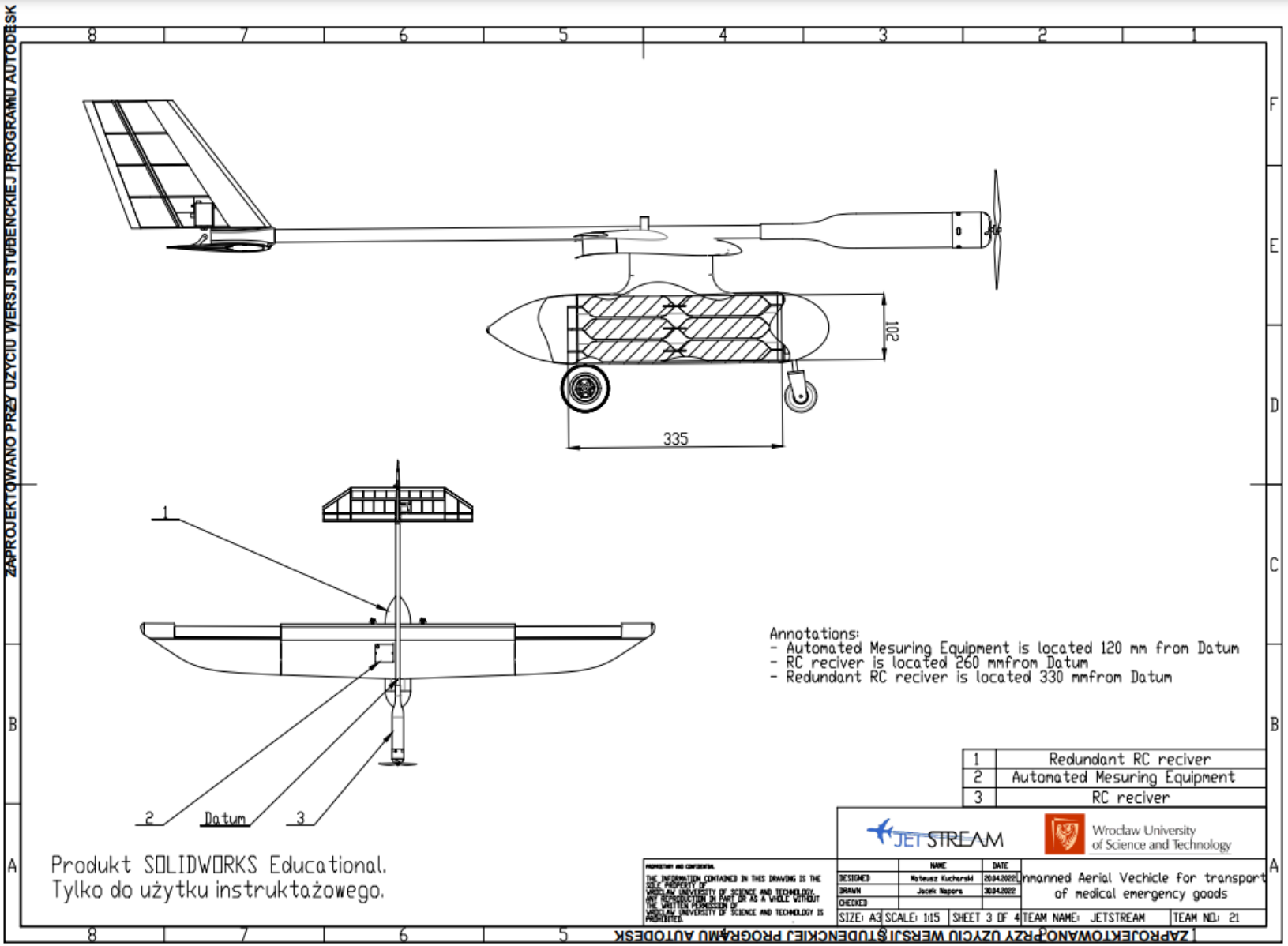
ZAPROJEKTOWANO PRZY UŻYCIU WERSJI STUDENCKIEJ PROGRAMU AUTODESK
335
202
1
2
Datum
3
Annotations:
- Automated Mesuring Equipment is located 120 mm from Datum
- RC reciver is located 260 mmfrom Datum
- Redundant RC reciver is located 330 mmfrom Datum
1 Redundant RC reciver
2 Automated Mesuring Equipment
3 RC reciver
JETSTREAM
Wrocław University of Science and Technology
Unmanned Aerial Vechicle for transport of medical emergency goods
SIZE: A3 SCALE: 1:15 SHEET 3 OF 4 TEAM NAME: JETSTREAM TEAM NO: 21
Produkt SOLIDWORKS Educational.
Tylko do użytku instruktażowego.

Datum is located on a center of a leading edge:
- MAC position is 29 mm from Datum
- Empty CG position is 101 mm from Datum, 43.90% MAC
- Fully loaded CG position is 109 mm from Datum, 47.38% MAC
- Fwd CG position is 5.90" from Datum, 31.30% MAC
- Aft CG position is 10.35" from Datum, 57.90% MAC
- Fwd stability margin is 1.58, 31.30%-39.68% MAC
- Aft stability margin is 2.87, 39.68%-57.90% MAC

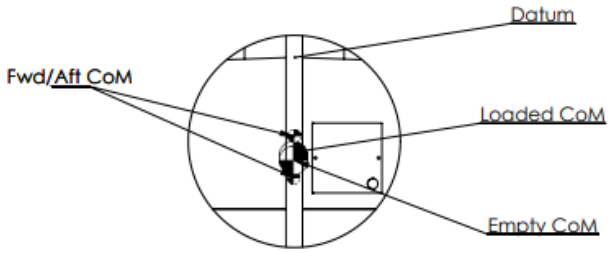

Detail
Scale 1 : 5

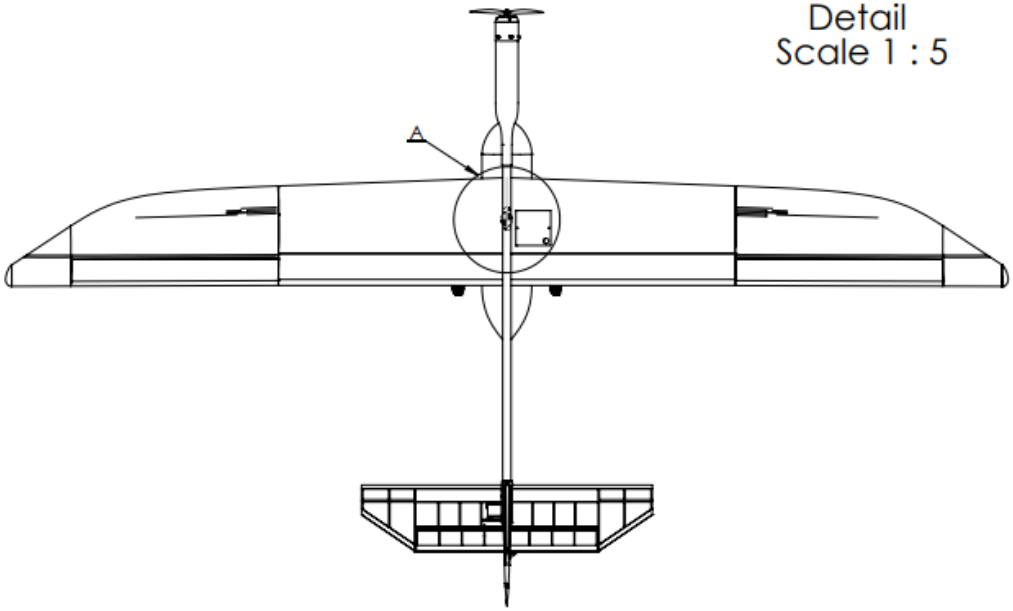

JETSTREAM

Wroclaw University of Science and Technology

	NAME	DATE
DESIGNED	Mateusz Kuchanski	20.04.2022
DRAWN	Jacek Napora	30.04.2022
CHECKED		

Unmanned Aerial Vechicle for transport of medical emergency goods

SIZE: A3 | SCALE: 1:8 | SHEET 4 OF 4 | TEAM NAME: **JETSTREAM** | TEAM NO.: **21**